



Discovery of Powerful Gamma-Ray Flares from the Crab Nebula

M. Tavani *et al.*

Science **331**, 736 (2011);

DOI: 10.1126/science.1200083

This copy is for your personal, non-commercial use only.

If you wish to distribute this article to others, you can order high-quality copies for your colleagues, clients, or customers by [clicking here](#).

Permission to republish or repurpose articles or portions of articles can be obtained by following the guidelines [here](#).

The following resources related to this article are available online at www.sciencemag.org (this information is current as of May 22, 2012):

Updated information and services, including high-resolution figures, can be found in the online version of this article at:

<http://www.sciencemag.org/content/331/6018/736.full.html>

Supporting Online Material can be found at:

<http://www.sciencemag.org/content/suppl/2011/01/03/science.1200083.DC1.html>

A list of selected additional articles on the Science Web sites **related to this article** can be found at:

<http://www.sciencemag.org/content/331/6018/736.full.html#related>

This article has been **cited by** 1 articles hosted by HighWire Press; see:

<http://www.sciencemag.org/content/331/6018/736.full.html#related-urls>

This article appears in the following **subject collections**:

Astronomy

<http://www.sciencemag.org/cgi/collection/astronomy>

30. T. Kaminishi *et al.*, *Structure* **15**, 289 (2007).
 31. A. Korostelev *et al.*, *Proc. Natl. Acad. Sci. U.S.A.* **104**, 16840 (2007).
 32. A. V. Komarova, L. S. Tchufistova, E. V. Supina, I. V. Boni, *RNA* **8**, 1137 (2002).
 33. J. Sengupta, R. K. Agrawal, J. Frank, *Proc. Natl. Acad. Sci. U.S.A.* **98**, 11991 (2001).
 34. M. A. Sørensen, J. Fricke, S. Pedersen, *J. Mol. Biol.* **280**, 561 (1998).
 35. B. T. Wimberly *et al.*, *Nature* **407**, 327 (2000).
 36. L. D. Kapp, J. R. Lorsch, *Annu. Rev. Biochem.* **73**, 657 (2004).
 37. M. Bycroft, T. J. P. Hubbard, M. Proctor, S. M. V. Freund, A. G. Murzin, *Cell* **88**, 235 (1997).
 38. L. Palm *et al.*, *J. Biol. Chem.* **270**, 6000 (1995).
 39. J. Nilsson, J. Sengupta, J. Frank, P. Nissen, *EMBO Rep.* **5**, 1137 (2004).
 40. T. Sunami *et al.*, *J. Biol. Chem.* **285**, 4587 (2010).
 41. K. Pachler *et al.*, *FEMS Yeast Res.* **5**, 271 (2004).
 42. N. Sang *et al.*, *J. Biol. Chem.* **276**, 27026 (2001).
 43. A. Gallina, F. Rossi, G. Milanesi, *Virology* **283**, 7 (2001).
 44. P. R. Smith *et al.*, *J. Virol.* **74**, 3082 (2000).
 45. J. Reinhardt, T. Wolff, *Vet. Microbiol.* **74**, 87 (2000).
 46. A. J. Link *et al.*, *Nat. Biotechnol.* **17**, 676 (1999).
 47. S. Baum, M. Bittins, S. Frey, M. Seedorf, *Biochem. J.* **380**, 823 (2004).
 48. P. A. Kiely *et al.*, *J. Biol. Chem.* **284**, 20263 (2009).
 49. D. Maag, J. R. Lorsch, *J. Mol. Biol.* **330**, 917 (2003).
 50. J. S. Nanda *et al.*, *J. Mol. Biol.* **394**, 268 (2009).
 51. Y. Yu *et al.*, *Nucleic Acids Res.* **37**, 5167 (2009).
 52. A. P. Carter *et al.*, *Science* **291**, 498 (2001); 10.1126/science.1057766.
 53. M. Selmer *et al.*, *Science* **313**, 1935 (2006); 10.1126/science.1131127.
 54. B. Castilho-Valavicius, H. Yoon, T. F. Donahue, *Genetics* **124**, 483 (1990).
 55. H. J. Yoon, T. F. Donahue, *Mol. Cell. Biol.* **12**, 248 (1992).
 56. Y. N. Cheung *et al.*, *Genes Dev.* **21**, 1217 (2007).
 57. A. Dallas, H. F. Noller, *Mol. Cell* **8**, 855 (2001).
 58. All data were collected at the Swiss Light Source (SLS, Paul Scherrer Institut, Villigen). We thank C. Schulze-Briese, A. Pauluhn, R. Bingel-Erlenmeyer, M. Müller, and T. Tomizaki for their outstanding support at the SLS; B. Blattmann from the NCCR crystallization facility for screening; R. Brunisholz for help with mass spectroscopy; N. Katheder, D. Baretic, and M. Weisser for their work during the initial phase of the project; S. Arpagaus for preparation of the material; T. Maier for advice during phasing; D. Böhlinger for critically reading the manuscript; all members of the Ban laboratory for suggestions and discussions; and A. Bringer for

providing a prerelease version of the CNS 1.3 refinement program. Supported by the Swiss National Science Foundation (SNSF), the National Center of Excellence in Research (NCCR) Structural Biology program of the SNSF, and European Research Council grant 250071 under the European Community's Seventh Framework Programme (N.B.), and the Max Rössler prize to N.B. Coordinates and structure factors have been deposited in the Protein Data Bank (PDB) with accession codes 2xzm and 2xzn. ETH Zürich has filed a patent application to use the crystals and the coordinates of the 40S ribosomal subunit for developing compounds that can interfere with eukaryotic translation.

Supporting Online Material

www.sciencemag.org/cgi/content/full/science.1198308/DC1
 Materials and Methods

SOM Text

Figs. S1 to S20

Tables S1 to S6

References

27 September 2010; accepted 15 December 2010

Published online 23 December 2010;

10.1126/science.1198308

REPORTS

Discovery of Powerful Gamma-Ray Flares from the Crab Nebula

M. Tavani,^{1,2,3,4*} A. Bulgarelli,⁵ V. Vittorini,¹ A. Pellizzoni,¹⁶ E. Striani,^{2,4} P. Caraveo,⁷ M. C. Weisskopf,²¹ A. Tennant,²¹ G. Pucella,⁶ A. Trois,¹ E. Costa,¹ Y. Evangelista,¹ C. Pittori,¹⁹ F. Verrecchia,¹⁹ E. Del Monte,¹ R. Campana,¹ M. Pilia,^{16,17} A. De Luca,^{7,25} I. Donnarumma,¹ D. Horns,²² C. Ferrigno,²³ C. O. Heinke,²⁴ M. Trifoglio,⁵ F. Gianotti,⁵ S. Vercellone,¹⁸ A. Argan,¹ G. Barbiellini,^{3,8,9} P. W. Cattaneo,¹⁰ A. W. Chen,^{3,7} T. Contessi,⁷ F. D'Ammando,¹⁸ G. DeParis,¹ G. Di Cocco,⁵ G. Di Persio,¹ M. Feroci,¹ A. Ferrari,^{3,11} M. Galli,¹² A. Giuliani,⁷ M. Giusti,^{1,3} C. Labanti,⁵ I. Lapshov,¹³ F. Lazzarotto,¹ P. Lipari,^{14,15} F. Longo,^{8,9} F. Fuschino,⁵ M. Marisaldi,⁵ S. Mereghetti,⁷ E. Morelli,⁵ E. Moretti,^{8,9} A. Morselli,⁴ L. Pacciani,¹ F. Perotti,⁷ G. Piano,^{1,4} P. Picozza,^{1,4} M. Prest,¹⁷ M. Rapisarda,⁶ A. Rappoldi,¹⁰ A. Rubini,¹ S. Sabatini,^{1,4} P. Soffitta,¹ E. Vallazza,⁹ A. Zambra,^{3,7} D. Zanello,^{14,15} F. Lucarelli,¹⁹ P. Santolamazza,¹⁹ P. Giommi,¹⁹ L. Salotti,²⁰ G. F. Bignami²⁵

The well-known Crab Nebula is at the center of the SN1054 supernova remnant. It consists of a rotationally powered pulsar interacting with a surrounding nebula through a relativistic particle wind. The emissions originating from the pulsar and nebula have been considered to be essentially stable. Here, we report the detection of strong gamma-ray (100 mega-electron volts to 10 giga-electron volts) flares observed by the AGILE satellite in September 2010 and October 2007. In both cases, the total gamma-ray flux increased by a factor of three compared with the non-flaring flux. The flare luminosity and short time scale favor an origin near the pulsar, and we discuss Chandra Observatory x-ray and Hubble Space Telescope optical follow-up observations of the nebula. Our observations challenge standard models of nebular emission and require power-law acceleration by shock-driven plasma wave turbulence within an approximately 1-day time scale.

The Crab Nebula (*I*) is a relic of a stellar explosion recorded by Chinese astronomers in 1054 A.D. It is located at a distance of 2 kpc from Earth and is energized by a powerful pulsar of spindown luminosity $L_{\text{PSR}} = 5 \times 10^{38}$ erg s⁻¹ and spin period $P = 33$ ms (2–4). Optical and x-ray images of the inner nebula show (*I*, 5–7) features such as “wisps” (composing a torus-shaped structure), “knots,” and the “anvil” [positioned along the South-East “jet”

originating from the pulsar and aligned with its rotation axis (6)]. Wisps, some of the knots, and the anvil are known to brighten and fade over weeks or months (6, 8). The Crab Nebula x-ray continuum and gamma rays up to ~100 MeV energies are modeled by means of synchrotron radiation and emission from giga- to teraelectron volt energies as inverse Compton radiation by accelerated electrons scattering cosmic microwave background (CMB) and nebular photons (9–12).

The AGILE (Astro-rivelatore Gamma a Immagini Leggero) satellite (*I3*) observed the Crab Nebula several times both in pointing mode from mid-2007 to mid-2009 and in spinning mode starting in November 2009 [supporting online material (SOM) text]. The AGILE instrument (*I3*)

¹Istituto Nazionale di Astrofisica—Istituto di Astrofisica Spaziale e Fisica Cosmica (INAF-IASF) Roma, via del Fosso del Cavaliere 100, 00133 Roma, Italy. ²Dipartimento di Fisica, Università degli Studi di Roma “Tor Vergata,” via della Ricerca Scientifica 1, 00133 Roma, Italy. ³Consorzio Interuniversitario Fisica Spaziale (CIFS), villa Gualino, v.le Settimio Severo 63, 10133 Torino, Italy. ⁴Istituto Nazionale di Fisica Nucleare (INFN) Roma Tor Vergata, via della Ricerca Scientifica 1, 00133 Roma, Italy. ⁵INAF-IASF Bologna, via Gobetti 101, 40129 Bologna, Italy. ⁶Ente per le Nuove tecnologie, l’Energia e l’Ambiente (ENEA) Frascati, via Enrico Fermi 45, 00044 Frascati(RM), Italy. ⁷INAF-IASF Milano, via E. Bassini 15, 20133 Milano, Italy. ⁸Dipartimento di Fisica, Università di Trieste, via A. Valerio 2, 34127 Trieste, Italy. ⁹INFN Trieste, Padriciano 99, 34012 Trieste, Italy. ¹⁰INFN Pavia, via Bassi 6, 27100 Pavia, Italy. ¹¹Dipartimento di Fisica Generale, Università degli Studi di Torino, via P. Giuria 1, 10125 Torino, Italy. ¹²ENEA Bologna, via don Fiammelli 2, 40128 Bologna, Italy. ¹³Space Research Institute, Russian Academy of Sciences, 84/32 Profsoyuznaya Street, 117997 Moscow, Russia. ¹⁴INFN Roma 1, p.le Aldo Moro 2, 00185 Roma, Italy. ¹⁵Dipartimento di Fisica, Università degli Studi di Roma “La Sapienza,” p.le Aldo Moro 2, 00185 Roma, Italy. ¹⁶INAF Osservatorio Astronomico di Cagliari, Poggio dei Pini, 09012 Capoterra, Italy. ¹⁷Dipartimento di Fisica, Università degli Studi dell’Insubria, via Valleggio 11, 22100, Como, Italy. ¹⁸INAF-IASF Palermo, via La Malfa 153, 90146 Palermo, Italy. ¹⁹Agenzia Spaziale Italiana (ASI) Science Data Center, European Space Agency (ESA) Centre for Earth Observation (ESRIN), 00044 Frascati, Italy. ²⁰ASI, viale Liegi 26, Roma, Italy. ²¹NASA, Marshall Space Flight Center, Huntsville, AL 35812, USA. ²²Institut fuer Experimentalphysik, University of Hamburg, Hamburg 22761, Germany. ²³Integral Science Data Centre, University of Geneva, Chemin d’Ecogia 16, CH-1290 Versoix, Switzerland. ²⁴Department of Physics, University of Alberta, Edmonton, Alberta T6G 2G7, Canada. ²⁵Istituto Universitario di Studi Superiori (IUSS), I-27100 Pavia, Italy.

*To whom correspondence should be addressed. E-mail: pi.agile@iasf-roma.inaf.it

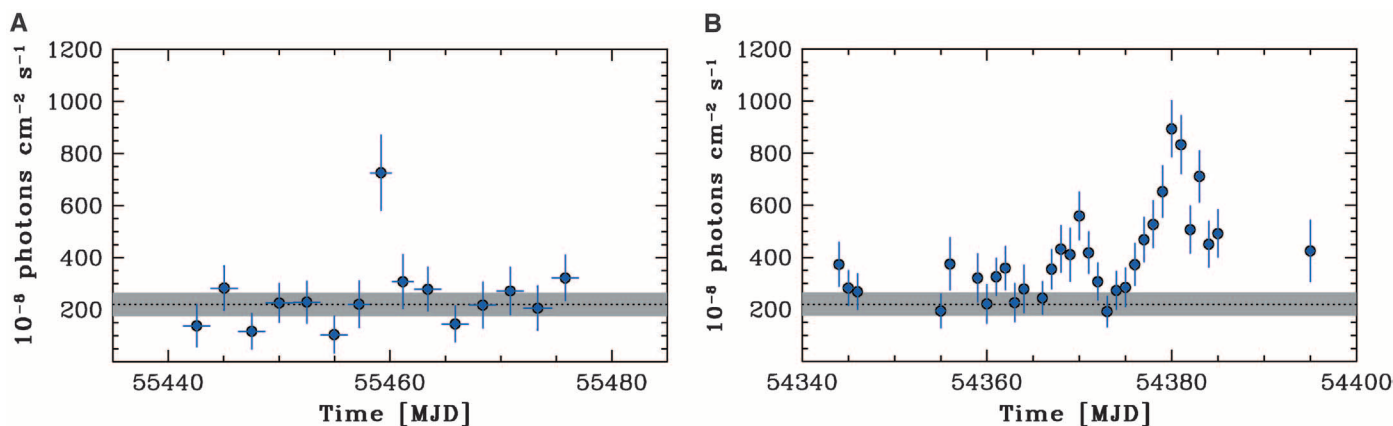
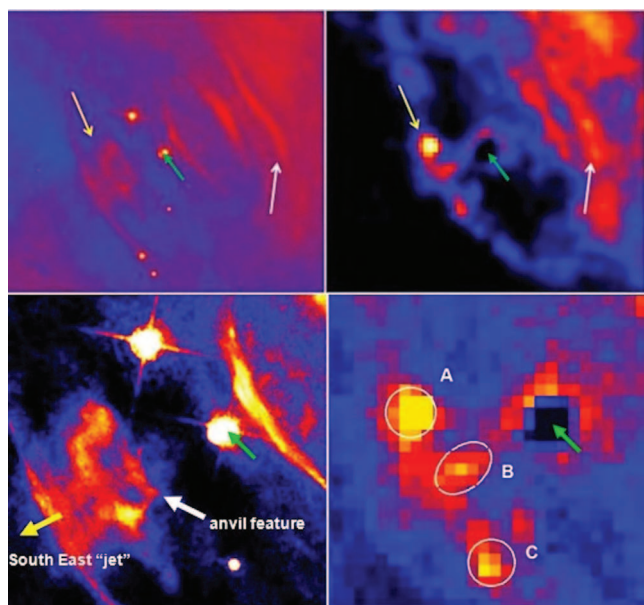


Fig. 1. Crab Nebula light curves of the total flux detected by AGILE in the energy range of 100 MeV to 5 GeV during the gamma-ray flaring periods in 2007 and 2010 (units of 10^{-8} photons cm^{-2} s^{-1}). **(A)** The “spinning” AGILE photon flux light curve during the period 2 September to 8 October 2010. Time bins are 2.5 days except near the flare peak (2-day binning). Errors are 1 SD, and time is given

in Modified Julian Day (MJD). The dotted line and gray band show the average Crab flux and the 3 SD uncertainty range. **(B)** The AGILE light curve during the period 27 September to 12 October 2007 (1-day binning) with the satellite in pointing mode. Errors are 1 SD. Time is given in MJD. The dotted line and gray band show the average Crab flux and the 3 SD uncertainty range.

Fig. 2. HST and Chandra imaging of the Crab Nebula after the September 2010 gamma-ray flare. (Top left) Optical image of the inner nebula region (approximately $28''$ by $28''$; north is up, east on the left) obtained by the Advanced Camera for Surveys (ACS) instrument on board the HST on 2 October 2010. ACS bandpass, 3500 to 11,000 Å. The pulsar position is marked with a green arrow in all panels. White arrows in all panels mark interesting features as compared with archival data. (Top right) The same region imaged by the Chandra Observatory Advanced CCD Imaging Spectrometer (ACIS) instrument on 28 September 2010 in the energy range of 0.5 to 8 keV (level-one data). The pulsar does not show in this map and below because of pileup.



(Bottom left) Zoom of the HST image (approximately $9''$ by $9''$), showing the nebular inner region, and the details of the anvil feature showing a ring-like structure at the base of the South-East jet off the pulsar. “Knot 1” at $0.6''$ southeast from the pulsar is saturated at the pulsar position. Terminology is from (6). (Bottom right) Zoom of the Chandra image, showing the x-ray brightening of the anvil region and the correspondence with the optical image. Analysis of the features marked A, B, and C gives the following results in the energy range of 0.5 to 8 keV for the flux F , spectral index α , and absorption N_{H} (quoted errors are statistical at the 68% confidence level): Feature A: flux $F = (48.5 \pm 8.7) \times 10^{-12}$ erg cm^{-2} s^{-1} , $\alpha = 1.76 \pm 0.30$, and $N_{\text{H}} = (0.36 \pm 0.05) \times 10^{22}$ atoms cm^{-2} ; Feature B: flux $F = (26.6 \pm 5.9) \times 10^{-12}$ erg cm^{-2} s^{-1} , $\alpha = 1.76 \pm 0.41$, and $N_{\text{H}} = (0.34 \pm 0.05) \times 10^{22}$ atoms cm^{-2} ; Feature C: flux $F = (25.3 \pm 5.9) \times 10^{-12}$ erg cm^{-2} s^{-1} , $\alpha = 1.46 \pm 0.36$, and $N_{\text{H}} = (0.34 \pm 0.04) \times 10^{22}$ atoms cm^{-2} .

monitors cosmic sources in the energy ranges from 100 MeV to 10 GeV (hereafter, GeV gamma-rays) and 18 to 60 keV with good sensitivity and angular resolution. With the exception of a remarkable episode in October 2007 (see below) we obtain, during standard nonactive states, an average (pulsar + nebula) flux value (14) of $F_{\text{g}} = (2.2 \pm 0.1) \times 10^{-6}$ photons cm^{-2} s^{-1} in the

range of 100 MeV to 5 GeV, for an average photon index $\alpha = 2.13 \pm 0.07$.

During routine monitoring in spinning mode in September 2010, a strong and unexpected gamma-ray flare, from the direction of the Crab Nebula was discovered (15) by AGILE at energies greater than 100 MeV. The flare reached its peak during 19–21 September 2010 with a 2-day

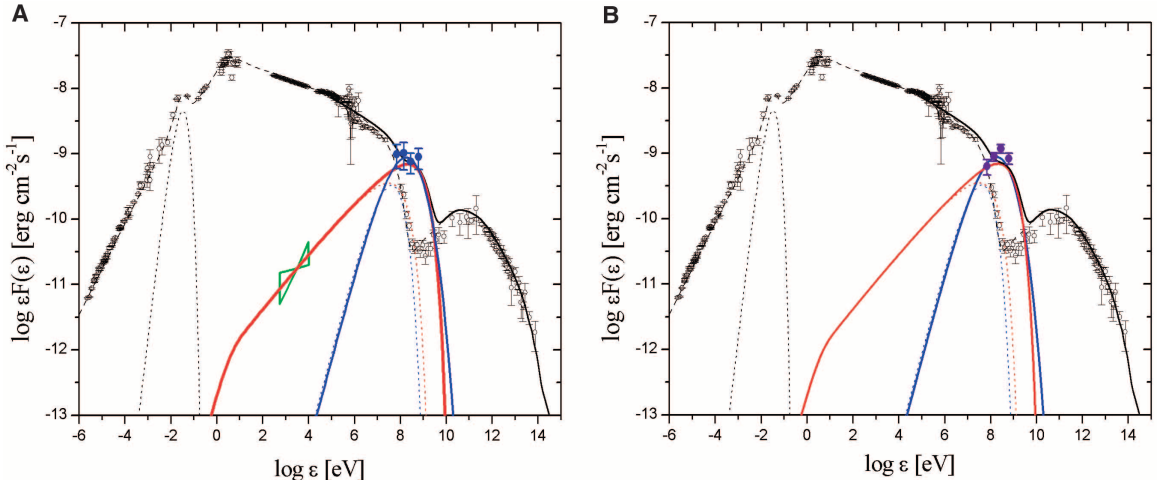
flux of $F_{\text{g,p1}} = (7.2 \pm 1.4) \times 10^{-6}$ photons cm^{-2} s^{-1} ($\alpha = 2.03 \pm 0.18$) for a 4.8 SD detection above the average flux. It subsequently decayed within 2 to 3 days to normal average values (Fig. 1A). This flare was independently confirmed by the Large Area Telescope (LAT) on board the Fermi Gamma-ray Space Telescope (Fermi) (16, 17), and different groups obtained multifrequency data in the following days (18). Recognizing the importance of this event was facilitated by a previous AGILE detection with similar characteristics.

AGILE detected another remarkable flare from the Crab in October 2007 (14). The flare extended for ~ 2 weeks and showed an interesting time substructure (Fig. 1B). The peak flux was reached on 7 October 2007, and the 1-day integration value was $F_{\text{g,p2}} = (8.9 \pm 1.1) \times 10^{-6}$ photons cm^{-2} s^{-1} ($\alpha = 2.05 \pm 0.13$) for a 6.2 SD detection above the standard flux.

For both the October 2007 and September 2010 events, there was no sign of variation of the pulsar gamma-ray signal (19–21) during and after these flares, as independently confirmed for the September 2010 event by means of gamma-ray (22), radio (23), and x-ray analyses (SOM text). We thus attribute both flares to unpulsed relativistic shock emission originating in the nebula.

Here, we focus on the September 2010 flare. Optical and x-ray imaging (18) show no additional source in the Crab region during and after the flare. The flaring giga-electron volt spectrum is substantially harder than the standard nebular emission (10–12). Figure 2 shows the high-resolution (arcsecond) optical and x-ray images of the nebula obtained 1 to 2 weeks after the flare by the Chandra Telescope and the Hubble Space Telescope (HST). A few nebular brightened features are noticeable in both images. The first one is the optical and x-ray anvil feature close to the base of the pulsar jet, which is a primary site of shocked particle acceleration in the inner neb-

Fig. 3. Spectral energy distribution of the Crab Nebula and the flaring gamma-ray episodes (the pulsar signal has been subtracted). Open black symbols indicate Crab Nebula emission in the steady state. The dashed curve shows our modeling of the steady state (1, 12, 21). The solid black curve shows our flare modeling for energies above 10^5 eV. The dotted black curve indicates nebular infrared emission (1). (A) Blue solid circles indicate spectral AGILE gamma-ray flare data integrated over 2 days (19–21 September 2010, MJD 55458.5 to 55460.5). Errors are 1 SD. Solid red and blue curves show the 2-day averaged spectral models according to synchrotron radiation from relativistic electrons/positrons impulsively accelerated in a shock region of size $L \leq 10^{16}$ cm. Dotted curves show the spectra evolved by synchrotron cooling 3 days after the flare. The blue curve model is based on a relativistic Maxwellian distribution of critical energy (Lorentz factor) $\gamma^* = 10^9$ (for a local $B = 10^{-3}$ G) representing the differential energy distribution of accelerated electrons. The red curve model is characterized (for a local $B = 10^{-3}$ G) by a double power-law electron differential distribution $dN(\gamma)/d\gamma = \gamma^{-p_1}$ for $\gamma_{\min} < \gamma < \gamma_{\text{break}}$



with $p_1 = 2.1$, $\gamma_{\min} = 5 \times 10^5$, $\gamma_{\text{break}} = 10^9$, and $dN(\gamma)/d\gamma = \gamma^{-p_2}$ for $\gamma_{\text{break}} < \gamma < \gamma_{\text{max}}$, with $p_2 = 2.7$, $\gamma_{\text{max}} = 7 \times 10^9$, and a total particle number $N_{e^-/e^+} = 10^{42}$. This model is extended toward the low-energy range and can account for the local x-ray spectral enhancements in the anvil region as observed by Chandra (Fig. 2). The area marked in green represents the 1 sSD x-ray spectral data for feature A of Fig. 2. (B) Violet symbols indicate spectral AGILE gamma-ray data during the 7–9 October 2007 flare (MJD 54380.5 to 54382.5). Errors are 1 SD. The black, blue, and red curves are those of the September 2010 flare and are shown here as a reference to compare the two spectra.

ula (6, 8). Another brightened feature is at a larger distance from the pulsar and appears as an elongated striation in both the HST and Chandra images.

Important constraints can be derived from the gamma-ray flare luminosity and time scale. The peak isotropic gamma-ray luminosity $L_p \approx 5 \times 10^{35}$ erg s $^{-1}$ implies for a 3 to 5% radiation efficiency (24–26) that about 2 to 3% of the total spindown pulsar luminosity was dissipated at the flaring site. This large value suggests that the production region was close to the pulsar. Also, the flare rise time (~ 1 day) favors a compact emission region of size $L \leq 10^{16}$ cm. The anvil feature is an excellent flare site candidate, also because of its alignment with the relativistic pulsar jet (1, 6, 8). This region is expected to be dominated by the leptonic current from the polar jets (24, 26).

Gamma-ray flaring from the Crab Nebula provides a new opportunity to constrain particle acceleration and radiative processes in a nebular environment. Synchrotron emission from a fresh population of shock-accelerated electrons/positrons along the pulsar polar jet can explain the flaring emission in the range of 0.1 to 10 GeV. Figure 3 shows our flare spectral data and two examples of modeling for different assumptions on the particle populations downstream of the shock (a pure electron-positron relativistic Maxwellian distribution and a distribution modified by a power-law component). Maxwellian and power-law models predict similar synchrotron radiation fluxes in the gigaelectron volt band, as shown in Fig. 3. However, if the emission from the anvil feature is related to the gamma-ray flaring then power-law models can explain also the x-ray

emission from that region. Fast cooling of the highest-energy particles drastically decreases the gigaelectron volt flux within a few days, as observed in both the September 2010 and October 2007 flares.

These gamma-ray flares test and constrain theoretical models applicable to pure pair plasmas (25–28) or to distributions modified by the presence of ions that resonantly accelerate pairs by magnetosonic waves (24, 26, 29). The acceleration rate resulting from local wave absorption at the relativistic (electron or ion) cyclotron frequency and from hydrodynamical constraints is determined to be $R_{\text{acc}} \sim (\text{day})^{-1}$, implying a flare region size of $L \approx 10^{16}$ cm for a standard downstream sound speed. Furthermore, reconciling the synchrotron cooling time scale $\tau \approx (8 \times 10^8 \text{ s}) B^{-2} \gamma^{-1}$ (where the magnetic field B is in gauss and γ is the particle Lorentz factor) with our observations implies, for a Lorentz factor $\gamma \approx 1 \times 10^9$ to 3×10^9 of electrons irradiating in the GeV range, a local magnetic field of $B \approx 10^{-3}$ G that is 3 to 10 times the nebular average (6, 12). Both the 2007 and 2010 gamma-ray flares have similar spectral characteristics (Fig. 3). These observations suggest that a common acceleration process produced electron/positron energy distributions with similar physical parameters.

Considering the AGILE exposure of the Crab Nebula, we estimate that one to two strong gamma-ray flares actually occur per year. The Crab Nebula is thus not a standard candle at gamma-ray energies. Variations of the Crab Nebula high-energy flux have also been recently reported at x-ray (30) and teraelectron volt (31) energies. It remains to be established whether the gamma-ray

flares that we report can be attributed to pulsar activity injecting fresh particles in the surroundings or to major plasma wave instabilities in the nebular environment.

References and Notes

1. J. J. Hester, *Annu. Rev. Astron. Astrophys.* **46**, 127 (2008).
2. M. J. Rees, J. E. Gunn, *Mon. Not. R. Astron. Soc.* **167**, 1 (1974).
3. M. Dobrowolny, A. Ferrari, *Astron. Astrophys.* **47**, 97 (1976).
4. C. F. Kennel, F. V. Coroniti, *Astrophys. J.* **283**, 710 (1984).
5. J. D. Scargle, *Astrophys. J.* **156**, 401 (1969).
6. J. J. Hester et al., *Astrophys. J.* **448**, 240 (1995).
7. M. C. Weisskopf et al., *Astrophys. J.* **536**, L81 (2000).
8. J. J. Hester et al., *Astrophys. J.* **577**, L49 (2002).
9. O. C. de Jager, A. K. Harding, *Astrophys. J.* **396**, 161 (1992).
10. O. C. de Jager et al., *Astrophys. J.* **457**, 253 (1996).
11. A. M. Atayan, F. A. Aharonian, *Mon. Not. R. Astron. Soc.* **278**, 525 (1996).
12. M. Meyer, D. Horns, H. S. Zechlin, *Astron. Astrophys.*, arXiv:1008.4524 (2010).
13. M. Tavani et al., *Astron. Astrophys.* **502**, 995 (2009).
14. C. Pittori et al., *Astron. Astrophys.* **506**, 1563 (2009).
15. M. Tavani et al., *Astronomer's Telegram*, 2855; www.astronomerstelegam.org (2010).
16. R. Buehler et al., *Astron. Telegram*, 2861; www.astronomerstelegam.org (2010).
17. A. A. Abdo et al., arXiv:1011.3855v1.
18. *Astronomer's Telegram*, 2856, 2858, 2866, 2867, 2868, 2872, 2879, 2882, 2889, 2893, 2903; www.astronomerstelegam.org (2010).
19. J. M. Fierro, P. F. Michelson, P. L. Nolan, D. J. Thompson, *Astrophys. J.* **494**, 734 (1998).
20. A. Pellizzoni et al., *Astrophys. J.* **691**, 1618 (2009).
21. A. A. Abdo et al., *Astrophys. J.* **708**, 1254 (2010).
22. E. Hays et al., *Astronomer's Telegram*, 2879; www.astronomerstelegam.org (2010).

23. C. M. Espinoza *et al.*, *Astronomer's Telegram*, 2889; www.astronomersteam.org (2010).
24. J. Arons, in *Neutron Stars and Pulsars, 40 Years After the Discovery*, W. Becker, Ed. (Springer, New York, 2008), pp. 1–56.
25. G. J. Kirk, A. W. Guthmann, Y. A. Gallant, A. Achteberg, *Astrophys. J.* **542**, 235 (2000).
26. A. Spitkovsky, A. Arons, *Astrophys. J.* **603**, 669 (2004).
27. U. Keshet, E. Waxman, *Phys. Rev. Lett.* **94**, 111102 (2005).
28. B. Reville, J. G. Kirk, *Astrophys. J.*, arXiv:1010.0872v1 (2010).
29. Y. A. Gallant, J. Arons, *Astrophys. J.* **435**, 230 (1994).
30. C. A. Wilson-Hodge *et al.*, arXiv:1010.2679v1 (2010).
31. G. Aielli *et al.*, *Astronomer's Telegram*, 2921; www.astronomersteam.org (2010).
32. We thank the Chandra Observatory Director H. Tananbaum; HST director M. Mountain; N. Gehrels; and the Swift team for their prompt response in carrying out the observations reported in this paper. Research partially supported by ASI grant I/089/06/2.

Supporting Online Material

www.sciencemag.org/cgi/content/full/science.1200083/DC1
SOM Text
Figs. S1 to S5
Table S1
References

21 October 2010; accepted 13 December 2010
Published online 6 January 2011;
10.1126/science.1200083

Gamma-Ray Flares from the Crab Nebula

A. A. Abdo,¹ M. Ackermann,² M. Ajello,² A. Allafort,² L. Baldini,³ J. Ballet,⁴ G. Barbiellini,^{5,6} D. Bastieri,^{7,8} K. Bechtol,² R. Bellazzini,³ B. Berenji,² R. D. Blandford,^{2*} E. D. Bloom,² E. Bonamente,^{9,10} A. W. Borgland,² A. Bouvier,² T. J. Brandt,^{11,12} J. Bregeon,³ A. Brez,³ M. Brigida,^{13,14} P. Bruel,¹⁵ R. Buehler,^{2*} S. Buson,^{7,8} G. A. Caliandro,¹⁶ R. A. Cameron,² A. Cannon,^{17,18} P. A. Caraveo,¹⁹ J. M. Casandjian,⁴ Ö. Çelik,^{17,20,21} E. Charles,² A. Chekhtman,²² C. C. Cheung,¹ J. Chiang,² S. Ciprini,¹⁰ R. Claus,² J. Cohen-Tanugi,²³ L. Costamante,² S. Cutini,²⁴ F. D'Ammando,^{25,26} C. D. Dermer,²⁷ A. de Angelis,²⁸ A. de Luca,²⁹ F. de Palma,^{13,14} S. W. Digel,² E. do Couto e Silva,² P. S. Drell,² A. Drlica-Wagner,² R. Dubois,² D. Dumora,³⁰ C. Favuzzi,^{13,14} S. J. Fegan,¹⁵ E. C. Ferrara,¹⁷ W. B. Focke,² P. Fortin,¹⁵ M. Frailis,^{28,31} Y. Fukazawa,³² S. Funk,^{2*} P. Fusco,^{13,14} F. Gargano,¹⁴ D. Gasparrini,²⁴ N. Gehrels,¹⁷ S. Germani,^{9,10} N. Giglietto,^{13,14} F. Giordano,^{13,14} M. Giroletti,³³ T. Glanzman,² G. Godfrey,² I. A. Grenier,⁴ M.-H. Grondin,³⁰ J. E. Grove,²⁷ S. Guiriec,³⁴ D. Hadasch,¹⁶ Y. Hanabata,³² A. K. Harding,¹⁷ K. Hayashi,³² M. Hayashida,² E. Hays,¹⁷ D. Horan,¹⁵ R. Itoh,³² G. Jóhannesson,³⁵ A. S. Johnson,² T. J. Johnson,^{17,36} D. Khagulyan,⁴² T. Kamae,² H. Katagiri,³² J. Kataoka,³⁷ M. Kerr,³⁸ J. Knödlseder,¹¹ M. Kuss,³ J. Lande,² L. Latronico,³ S.-H. Lee,² M. Lemoine-Goumard,³⁰ F. Longo,^{5,6} F. Loparco,^{13,14} P. Lubrano,^{9,10} G. M. Madejski,² A. Makeev,²² M. Marelli,¹⁹ M. N. Mazziotta,¹⁴ J. E. McEnery,^{17,36} P. F. Michelson,² W. Mitthumsiri,² T. Mizuno,³² A. A. Moiseev,^{20,36} C. Monte,^{13,14} M. E. Monzani,² A. Morselli,³⁹ I. V. Moskalenko,² S. Murgia,² T. Nakamori,³⁷ M. Naumann-Godo,⁴ P. L. Nolan,² J. P. Norris,⁴⁰ E. Nuss,²³ T. Ohsugi,⁴¹ A. Okumura,⁴² N. Omodei,² J. F. Ormes,⁴⁰ M. Ozaki,⁴² D. Paneque,² D. Parent,²² V. Pelassa,²³ M. Pepe,^{9,10} M. Pesce-Rollins,³ M. Pierbattista,⁴ F. Piron,²³ T. A. Porter,² S. Rainò,^{13,14} R. Rando,^{7,8} P. S. Ray,²⁷ M. Razzano,³ A. Reimer,^{2,43} O. Reimer,^{2,43} T. Reposeur,³⁰ S. Ritz,⁴⁴ R. W. Romani,² H. F.-W. Sadrozinski,⁴⁴ D. Sanchez,¹⁵ P. M. Saz Parkinson,⁴⁴ J. D. Scargle,⁴⁵ T. L. Schalk,⁴⁴ C. Sgrò,³ E. J. Siskind,⁴⁶ P. D. Smith,¹² G. Spandre,³ P. Spinelli,^{13,14} M. S. Strickman,²⁷ D. J. Suson,⁴⁷ H. Takahashi,⁴¹ T. Takahashi,⁴² T. Tanaka,² J. B. Thayer,² D. J. Thompson,¹⁷ L. Tibaldo,^{4,7,8} D. F. Torres,^{16,48} G. Tosti,^{9,10} A. Tramacere,^{2,49,50} E. Troja,¹⁷ Y. Uchiyama,² J. Vandenbroucke,² V. Vasileiou,^{20,21} G. Vianello,^{2,49} V. Vitale,^{39,51} P. Wang,² K. S. Wood,²⁷ Z. Yang,^{52,53} M. Ziegler⁴⁴

A young and energetic pulsar powers the well-known Crab Nebula. Here, we describe two separate gamma-ray (photon energy greater than 100 mega-electron volts) flares from this source detected by the Large Area Telescope on board the Fermi Gamma-ray Space Telescope. The first flare occurred in February 2009 and lasted approximately 16 days. The second flare was detected in September 2010 and lasted approximately 4 days. During these outbursts, the gamma-ray flux from the nebula increased by factors of four and six, respectively. The brevity of the flares implies that the gamma rays were emitted via synchrotron radiation from peta-electron-volt (10^{15} electron volts) electrons in a region smaller than 1.4×10^{-2} parsecs. These are the highest-energy particles that can be associated with a discrete astronomical source, and they pose challenges to particle acceleration theory.

The Crab Nebula is the remnant of an historical supernova (SN), recorded in 1054 A.D., located at a distance of 2 kpc (*1*). The SN explosion left behind a pulsar, which continuously emits a wind of magnetized plasma of electron/positron pairs (henceforth referred to as electrons). This pulsar wind is expected to terminate in a standing shock, in which the particles may undergo shock acceleration (*2, 3*). As the electrons diffuse into the downstream medi-

um, they release energy through interactions with the surrounding magnetic and photon fields. This emission is observed across all wavebands, from radio up to teraelectron-volt gamma-ray energies and is referred to as a pulsar wind nebula (PWN). The efficiency of this process is remarkable. As much as 30% of the total energy released by the Crab pulsar is emitted by the PWN [*4*] and references therein]. The Crab PWN has an approximately ellipsoidal shape on the sky with a

size that decreases with increasing photon energy. At radio frequencies, it extends out to $5'$ (3 pc) from the central pulsar. At x-ray wavelengths, a bright torus surrounds the pulsar; its radius is $40''$ (0.4 pc), and jets emerge perpendicular to it in both directions.

Within the region encapsulated by the torus, there are several small-scale structures. The inner nebula, which we define as the central $15''$ around the pulsar, has several small-scale regions of variable x-ray and optical brightness. The most prominent is an x-ray-bright inner ring with a radius of $10''$ (0.1 pc); this ring is thought to represent the termination shock of the PWN (*5*). Several knots with diameters of $\sim 1''$ (0.01 pc) are detected close to the inner ring and the base of the jets, and bright arcs of comparable width are observed moving outwards from the inner ring into the torus (*6, 7*).

The broad-band spectral energy distribution (SED) of the Crab Nebula is composed of two broad nonthermal components. A low-energy component dominates the overall output and extends from radio to gamma-ray frequencies. This emission is thought to be from synchrotron radiation. This notion is confirmed in radio to x-ray frequencies through polarization measurements (*8–10*). The emission of this synchrotron component peaks between optical and x-ray frequencies, where the emission is primarily from the torus (*5*). The emission site of higher-energy photons (beyond 100 keV) cannot be resolved because of the limited angular resolution of telescopes that are observing at these frequencies. The high-energy component dominates the emission above ~ 400 MeV and is thought to be emitted via inverse Compton (IC) scattering, predominantly of the synchrotron photons (*11, 12*).

The large-scale integrated emission from the Crab Nebula is expected to be steady within a few percent and is thus often used to cross-calibrate x-ray and gamma-ray telescopes and to check their stability over time (*13, 14*). Recently, variability in the x-ray flux from the nebula by $\sim 3.5\%$ year⁻¹ has been detected, setting limits on the accuracy of this practice (*15*). Yearly variations in the emission in the high-energy tail (1 to 150 MeV) of the synchrotron component has also been reported (*16, 17*). No significant variations have been detected for the high-energy component of the nebula (*18–20*).

The Large Area Telescope (LAT) on board the Fermi Gamma-Ray Space Telescope (Fermi) has continuously monitored the Crab Nebula as a